Chapter 2
Amplitude Modulated Mode-Locked Figure Eight Fiber Laser

As mentioned in Chapter 1, the development of mode-locked fiber laser can apply the long-distance fiber transmission. We purpose design an active mode-locked fiber laser using amplitude modulator to lock higher frequency pulse train. This Chapter is organized as follows: Section 2-1 introduces the mode-locked figure eight fiber laser(MLF8L). The structure of MLF8L is described in Section 2-2. We derive the theoretical model using ABCD matrix in Section 2-3. In Section 2-4, we present the experimental results. We also give the summary and discussions of our designed MLF8L in Section 2-5.

2-1 Introduction

Optical fiber amplifiers are the important key components in optical sources[32], optical transmission systems[33] and optical networks. In 1985 year, the Pools *et al* published the technique of doping rare earth elements in fiber and finish product of the first erbium-doped fiber amplifier(EDFA) [34]. Because advantages of the low loss wavelength

range in C band, people attach importance to the applications of EDFA. The EDFA have the advantages of high gain(>17 dB), high output power(>20 dBm), low noise figure(4~6 dB) and polarization independent. The EDFA fit in signals of various transmission speed and different modulated form.

Much research has been devoted to obtaining short pulses at high repetition rates. Most of this effort has centered on meeting the stringent requirements of future high-speed optical communication systems [35]. Another important use of short-pulse high-repetition-rate lasers with somewhat different requirements, is in nonlinear optical experiments. One of the major problems encountered in nonlinear experiments with short pulses is the convolution of low frequency spurious noise into the spectral window of the measurement apparatus [36]. This problem is especially serious in squeezing experiments in optical fibers where the guided acoustic wave Brillouin scattering (GAWBS) induces phase and polarization modulation and obscures the squeezing effects [37]. One of the methods to combat the convolution of the low frequency noise into the measurement window is to employ a high-frequency short-pulse source [38]. For these experiments the choice of pulse rate is a compromise between the noise limitations and the pulse energy requirement. In most cases, sources with a rate of 1–2 GHz are the ideal solution. Short pulse generation at this repetition rate poses a unique challenge since the soliton compression techniques employed at 10-GHz rates are less applicable to obtaining subpicosecond pulses at1 GHz.To achieve operation at high repetition rate either the cavity of the laser is made as short as possible or the laser is induced to operate at a

multiple of the basic repetition rate. This latter method of operation is termed harmonic mode-locking. For solid-state lasers, a short-cavity design resulting in cavity repetition rates of 1 GHz has been demonstrated in [39]. While the shortest fiber laser reported [40] had a basic repetition rate of 290 MHz, with harmonic mode-locking this laser could emit pulses at up to 2.7 GHz. Harmonic mode-locking has been demonstrated using pulse self-ordering [41], delayed feedback [42] and active modelocking [43].

The first proposition of mode-locking appear by the research of Gürs and Müller[41] on ruby lasers. The first papers clearly identifying the mechanism published in 1964 by DiDomenico[42], Hargrove *et al* [43], and Yariv[44]. The case of active mode-locked is that Hargrove *et al* achieved mode-locking by internal loss modulation inside the resonator. Mocker and Collins[45] showed that the saturable dye used in ruby lasers to Q-switch the laser could also be used to be mode-locking. Q-switching is a process in which the laser is caused to emit pulses that are many roundtrips in duration. The saturation absorber is bleached by the radiation in the resonator. The emission of radiation stops when the gain medium is depleted, and the process starts all over again. Mocker and Collins observed that the Q-switched pulse broke up into a train of very short pulses separated by the roundtrip time. The train carried the same energy as the Q-switched pulse and hence the pulses were of much greater peak intensity than the pulses produced by Q-switching alone. That was the first example of passive mode-locking. For several years, techniques were developed for measurement of these pulses and for their use to probe nonlinear response of optical media. The measurement

accuracy was impaired by the somewhat unpredictable nature of the transient mode-locking. This drawback was overcome when Ippen *et al*[46] generated the first CW saturable absorber mode-locking. Shortly thereafter this led to production of pulses of sub-picosecond duration[47]. The reproducible character of these pulses improved the accuracy of pump-probe measurements by four orders of magnitude. The work continued unabated for the next decade producing shorter and shorter pulses[48-50]. Ultimately, a record 6-fs pulse duration was achieved by Fork *et al* using pulse compression external to the cavity[51]. The pulse compression technique uses the Kerr nonlinearity of an optical medium. The pulses propagating through the medium with nonlinear phase shifts that induce spectral broadening and pulse compressing.

The analytic theory of active mode-locking was firmly established in a classic paper by Siegman and Kuizenga[52]. The soliton laser[53] consisted of two resonators, one active the other passive and containing a fiber, coupled via a semitransparent mirror to the laser resonator. The two resonators were feedback stabilized to within a fraction of a wavelength. The operation of this laser was explained afterwards as an interference phenomenon between the pulses circulating in the two subresonators and interfering at the semitransparent mirror[54]. Through proper phasing a net pulse shaping is produced analogous to that of a fast saturable absorber. The process was dubbed additive pulse mode-locking(APM)[55]. The principle was generalized to fiber ring lasers in which the APM action is produced by a birefringent element in the resonator. Via polarization controllers the pulse is split into two co-propagating versions in the fiber.

The interference of the two polarizations at the output polarizer leads to effective fast-saturable-absorber action.

The Kerr-lens mode-locking(KLM) were written by several laboratories[56-59]. The effect of a fast saturable absorber is simulated by Kerr focusing: the high intensity part of the beam is focused by the Kerr–effect, whereas the low intensity parts remain unfocused. If such a beam is passed through an aperture, the low intensity parts are attenuated, thereby shortening the pulse.

There is another variant of this pulse shaping by the Kerr–effect and dispersion, in a way analogous to dispersion-managed soliton propagation[60]. The dispersion in the ring may be made to vary from normal to anomalous by proper splicing of fiber segments. The pulse inside the resonator stretches and compresses[61]. The net dispersion may be zero, yet soliton-like pulse shaping is still possible[62]. The reason for this is the fiber nonlinearity that causes the pulse spectrum to be narrower in the segment with normal dispersion than in the segment with anomalous dispersion. Thus, on the average, the pulse experiences anomalous dispersion which balances the Kerr-effect.

The continuous wave(CW) light coming out of a laser cavity consists of a range of longitudinal modes with random phase relative phases. When the relative phases between these different longitudinal modes of the laser cavity are locked to a constant value, the laser generates a periodic pulse output. This technique is known as mode-locking. A continuous wave erbium ring laser can be actively mode-locked by using an amplitude or

phase modulator[63,64] to generate pulses at the modulation frequency f_m ,where

$$f_m = f_c = \frac{c}{nL} \tag{2-1}$$

where f_c is the cavity free spectral range(FSR), c is the speed of light, L is the cavity length and n is the refractive index of the cavity . These pulses have a round trip time of t_p, which is related to f_c and the pulsewidth τ by

$$N = \frac{1}{f_m \tau} \tag{2-2}$$

N is the total number of longitudinal modes in the cavity [65].

In order to increase the pulse repetition rate, pulses could be produced at integer harmonic of the cavity mode-spacing by modulation frequency f_m, given by

$$f_m = pf_p \tag{2-3}$$

p is an integer representing the number of longitudinal modes locked, and ranges from a few hundred to tens of thousand.

The Kuizenga and Siegman theory[66] predicts that with AM mode-locking the time bandwidth product is 0.44 for a chirp-free Gaussian pulse and 0.315 for a Sech pulse. Furthermore, it states that the pulse width

τ is inversely proportional to $(\delta)^{1/4}$and $(f_m \Delta f)^{1/2}$, so that

$$\tau = K(\frac{1}{f_m \Delta f})^{\frac{1}{2}}(\frac{1}{\delta})^{\frac{1}{4}} \qquad (2\text{-}4)$$

Here δ is the effective single-pass amplitude modulation depth, Δf is the gain bandwidth of the laser cavity and K is a pulse shape-dependent constant. Therefore, with increasing modulation frequency and increasing modulation amplitude level, the pulsewidth of output can be shorter.

Ahmed and Onodera[67] introduced the idea of mode-locking a laser cavity at rational harmonics of the modulator frequency to generate pulse train of higher repetition rate. This is achieved by slightly detuning the cavity frequency f_c so that it is now related to the modulator frequency f_m by[68,69]

$$f_m = (p \pm \frac{1}{k}) f_c \qquad (2\text{-}5)$$

This leads to a pulse repetition rate of f_p, given by

$$f_p = (kp \pm 1) f_c \qquad (2\text{-}6)$$

Therefore , rationally mode-lock ring lasers generate optical pulses at a repetition rate that is k time greater than the modulator frequency.

Rational mode-locking of erbium-doped fiber lasers at repetition rates of up to 200 GHz have been reported [70.71].

Many kinds of all-optical switching elements such as a nonlinear amplified loop mirror (NALM)[72,73], a nonlinear optical loop mirror (NOLM)[74-75], and a nonlinear polarization rotator have been investigated extensively lately. These devices are useful for generation of ultrashort optical pulses, all-optical demultiplexing, pedestal suppression of pulses, and so on.

Both of optical time division multiplexing(OTDM) and wavelength division multiplexing(WDM) could be used for extending the capacity of communication system. When the density of the used wavelengths between two near channels is higher and higher in the future, the crosstalk between two wavelength channels will become more serious. Oppositely, OTDM can fully being used in high speed multiplexing. The mode-locked laser is a good technique which can generate short pulse and high power intensity for high speed systems. Laser mode-locking can be classified as active and passive types. Active mode-locked laser is easier to achieve high repetition rate rather than passive mode-locked laser. Active mode-locked laser is able to be adjusted by triggering certain signal to generate harmonic and rational mode-locked laser light output. The repetition rate of pulse trains generated by passive mode-locked laser are mainly controlled with the intracavity properties of component. Among a lot of fiber mode-locked laser structure, figure eight laser(F8L) is one of the famous active mode-locked laser[76-79].

The structure of mode-locked figure eight fiber laser(MLF8L) was first demonstrated by Duling III[80] to provide clear linear and nonlinear area of light traveling in cavity. Some important controlling factors of mode-locked F8L, for example coupling coefficient of central coupler, has been researched by some groups[81]. Such technique can be applied on measurement system[82,83] to ensure the high sampling rate. Besides, because the requirements of speed and capacity of communication go high, many researches also have reported related fiber laser for applying in high speed photonic systems[84,85].

2-2 System Description

In this Section, we design a MLF8L system as shown in Fig. 2-1. With tuning the modulation frequency from 10GHz to 12.5GHz voltage controllered oscillatiors(VCO), we find the fundamental mode locking is 2.5 MHz. Following formula of the free spectral range(FSR): $FSR = \frac{c}{nL}$, where the n is 1.46, the c is velocity of light and L is the cavity length, we find the cavity length about 82.19 m.

The components include a EDFAs(Lightwave Link, 19”Rack mount, model no. EDFA-1700H), a polarization controllers(PC), an isolator, a amplitude modulator(JDS Uniphase Corporation, model no.424535), a VCO(EMF Systems Inc, model no.515085), a mixer(WJ Corporation,

model no.M86C), a network analyzer(HP, model no.5150858510C) and two couplers. The right side of this system is a nonlinear amplified loop mirror(NALM) which can effectively compress the pulse amplified the power[86,87]. We use EDFAs to be the gain medium in cavity to get higher power of output port and can enhance nonlinear Kerr effect as the nonlinear refraction index as

$$n = n_0 - n_2 I(t) \tag{2-7}$$

where n_0 is the linear refractive index, n_2 is nonlinear coefficient and $I(t)$ is the light intensity. The EDFA have gains of 20 dB. The effect on using unbalanced coupler has been demonstrated[88]. The advantage of using unbalanced central coupler is reducing the power loss in ring cavity.

In the left side, we set an isolator to reduce the light coming from the 10% counterclockwise light wave to prevent interfere. The EDFA in the right side loop of the F8L also have isolators inside to suppress the counterclockwise light propagation. Besides, we use an amplitude modulator to generate the active mode locking. The amplitude mode-locked laser for change of amplitude is very sensitivity. We directly to control and tuning the amplitude change by amplitude modulator. The amplitude modulator with external adding the bias voltage can easily generate high quality of harmonic and rational mode-locked laser. The PC is used to tune the polarization state in this system. With properly control the condition of polarization in F8L cavity, we can have a better output pulses. In this paper, we give 10GHz radio frequency(RF) signal to modulate the amplitude

modulator. When we adjust frequency of amplitude modulator, the pulsewidth of the laser can be varied. A 3 dB 2x2 coupler at last is connected to a high speed sampling oscilloscope to see the pulse time response. The another port of 3 dB coupler use matching index oil to avoid the light reflection because of different index between core and air.

2-3 Theoretical Model

In this Section, we use the time-domain ABCD matrix to analyze MLF8L. The time-domain ABCD matrix formalism for mode-locked laser was developed by M. Nakazawa *et al*[89]. The basic of ABCD matrix is set on the Haus's notation[90]. The time-domain ABCD matrix can apply to AM mode-locked situations, FM mode-locked laser and so on. After Nakazawa *et al* proposed, there are some groups to improve and expand the model[91]. They consider the practical conditions to add some factors like dispersion and nonlinear in fiber and in laser cavity to make the formulism more complete.

2-3-1 Time-Domain ABCD Matrix

The parameter, which is the complex radius of curvature of a Hermite–Gaussian beam, is characterized by

$$\frac{1}{q} = \frac{1}{R} - i\frac{\lambda}{\pi w_s^{\,2}} \tag{2-8}$$

where R and w_s are the radius of curvature and the Gaussian spot size, respectively. When such a beam passes through an optical element characterized by an matrix, the parameter at the output satisfies

$$q_{out} = \frac{Aq_{in} + B}{Cq_{in} + D} \tag{2-9}$$

where we have the following relationship:

$$AD - BC = 1 \tag{2-10}$$

These spatial parameters can be transformed into parameters in the time domain when the propagating pulse is characterized as a chirped Gaussian pulse. It is possible to exchange the radial direction with time. In this case, for Gaussian pulse propagation in the time domain, a new parameter can be defined by

$$\frac{1}{q} = \frac{1 + iC}{\tau^{\,2}} \tag{2-11}$$

where τ is the pulsewidth of the intensity and C is the chirp at a given

position. By comparing Eq. (2-11) with Eq. (2-8), the spot size which is expressed as an imaginary part of Eq. (2-8), as corresponding to the pulsewidth, which is expressed as the real part of Eq. (2-11). This conversion makes it easy to understand the time-domain matrix with its elements as detailed below. The Gaussian pulse propagation in a dispersive medium is given by

$$\frac{\partial A}{\partial z} = i\frac{1}{2}\beta'' \frac{\partial^2}{\partial t^2} A \tag{2-12}$$

Here β'' is the second-order dispersion. A matrix in the time domain after passing through a dispersive medium is given by

$$\begin{pmatrix} 1 & -i\beta'' L \\ 0 & 1 \end{pmatrix} \tag{2-13}$$

where L is the length of dispersion medium.

2-3-2 Theoretical Model of A Amplitude Modulated MLF8L

The diagram of our designed ABCD matrix system is shown in Fig. 2-2. This system mainly is combined by three elements: the phase modulator, the EDFA, fiber dispersion and nonlinearity. We can regard the EDFA as the dispersion and nonlinearity of erbium-doped fiber(EDF). All

of components are shown in Table 2-2[92]. The ABCD matrices of amplitude modulator is $\begin{pmatrix} 1 & 0 \\ 4\pi^2 mf^2 & 1 \end{pmatrix}$, the EDFA is $\prod_{j=1}^{N}\begin{pmatrix} 1 & 0 \\ i\frac{2r_E\overline{P}L_E}{N\sqrt{\pi}f\tau^3(j)} & 1 \end{pmatrix}\begin{pmatrix} 1 & -\frac{i\beta_E'' L_E}{N} \\ 0 & 1 \end{pmatrix}$, and the single-mode fiber(SMF) is $\prod_{i=1}^{M}\begin{pmatrix} 1 & 0 \\ i\frac{2r_S\overline{P}L_S}{M\sqrt{\pi}f\tau^3(i)} & 1 \end{pmatrix}\begin{pmatrix} 1 & -\frac{i\beta_S'' L_S}{M} \\ 0 & 1 \end{pmatrix}$. The m is the modulation depth, f is the modulation frequency, β'' is second-order dispersion, L_E and L_s are the propagation distance in SMF and EDF, and $\overline{P}$ is the average power in cavity. The second-order dispersion can express by

$$\beta'' = -\frac{\lambda^2}{2\pi c}D \tag{2-14}$$

where the D is group velocity dispersion(GVD) and λ is the central wavelength. The connection between the peak power P_0 and the mean power $\overline{P}$ can be presented by[72]

$$\overline{P} = \sqrt{\pi} f\tau\, P_0 \tag{2-15}$$

When a mode-locked laser cavity consists of several optical elements, one can immediately obtain a steady-state solution of a mode-locked pulse by using the relationship $\frac{1}{q(0)} = \frac{1}{q(L_T)}$ in time-domain ABCD matrix.

Here L_T is the cavity length. Thus[92],

$$\frac{1}{q}=\frac{D_T-A_T\pm\sqrt{\left(A_T-D_T\right)^2+4B_TC_T}}{2B_T} \tag{2-16}$$

The MLF8L can look on as a phase modulator to link the EDFA, to go through the block of SMF as shown in Fig. 2-2. Thus, the overall ABCD matrix for a phase modulated MLF8L can be expressed by

$$\begin{pmatrix} A_T & B_T \\ C_T & D_T \end{pmatrix}=\begin{pmatrix} 1 & 0 \\ 4\pi^2 mf^2 & 1 \end{pmatrix}\times \prod_{j=1}^{M}\begin{pmatrix} 1 & 0 \\ i\dfrac{2r_E\overline{P}L_E}{N\sqrt{\pi}f\tau^3(j)} & 1 \end{pmatrix}\begin{pmatrix} 1 & -\dfrac{i\beta_E''L_E}{N} \\ 0 & 1 \end{pmatrix}\times \prod_{i=1}^{N}\begin{pmatrix} 1 & 0 \\ i\dfrac{2r_S\overline{P}L_S}{M\sqrt{\pi}f\tau^3(i)} & 1 \end{pmatrix}\begin{pmatrix} 1 & -\dfrac{i\beta_S''L_S}{M} \\ 0 & 1 \end{pmatrix} \tag{2-17}$$

We have to solute the Eq. (2-17). Then, the Eq. (2-17) substitutes the $\begin{pmatrix} A_T & B_T \\ C_T & D_T \end{pmatrix}$ in Eq. (2-16). We can get the pulsewidth and chirp parameter of MLF8L with solute Eq (2-16) and Eq (2-11). The detailed derivation of SMF can be represented as Appendix A. From the Eq. (A-13) to (A-17), the results are so complex that we can't easily solute the analytic solution. The matixs of multiplying amplitude modulator, EDFA, and SMF can utilize

software of Mathematica to calculate the approximate value. The total parameters are listed in Table 2-3. The simulation results are shown in Fig. 2-3 and Fig. 2-4. We describe in next Section.

2-4 Analysis of Results

We used the structure of MLF8L not only get the nice output, but also analyze the results of detuning the modulation frequency. We have tried to adjust the modulation frequency to observe the change of pulse trains. Fig. 2-3 depicts the theoretical and experimental results. From observing the theory curve(solid line), we find the range of pulsewidth of 22.52 ps to 17.58 ps following modulation frequency to display two order decay. This is easily to understand by Eq. (2-17), although we can't solute the analytic solution. Of course, if we use different parameters in other elements, the curvature may be shifted or change, but the trends of two order decay following the modulation frequency to become large. In Fig. 2-3, we have proved the theoretical and experimental curves are very close. We also can depict the theoretical chirp parameter of our designed MLF8L in Fig. 2-4. At modulation frequency is 10 GHz, the pulsewidth is 22.52 ps and the chirp parameter is about -88.3879. The chirp parameters vary with modulation frequency from 10 GHz to 12.5 GHz are within -66.032.

In next subsection, we use the modulation frequency(MF) of 10 GHz and amplitude level(AL) of 16.4 dBm to generate 10 Gb/s pulse train.

2-4-1 10 GHz Pulse Train Generation

We use Agilent 86100A high speed sampling oscilloscope to measure the time response of MLF8L. When tuning the frequency of 1 times fundamental MF, the first order harmonic mode-locked laser is generated as shown in Fig. 2-5. This lasing spectrum is shown in Fig. 2-6. The bandwidth of lasing spectrum is 6 nm.

The variation of the repetition rate by detuning MF is shown in Fig. 2-7. The largest value 10.00002 GHz of repetition rate at MF of 10 GHz and amplitude level of 16.4 dBm. Besides, we find the maximum change range is 0.0047 GHz at AL of 16.4 dBm.

Fig. 2-8 depicted the curve of MF versus pulsewidth. In our experimental results, the pulsewidths become broaden when far away MF of 10.000126 GHz.

The rise time and falling time are the important parameters of pulse shapes. The rise time, falling time and pulsewidth can directly affect the bit error rate because of intersymbol interference. Thus, we have to understand the change of pulse. The rise time and falling time vary with MF as shown in Fig 2-9 and Fig 2-10, respectively. The rise time become flat when MF are far away 10.000126 GHz. Oppositely, the falling time can be sharper. The root-mean-spuare(RMS) jitter become worse except 10.000126 GHz as shown in Fig. 2-11. At The worst RMS jitter is 10.52 ps, and the optimal

RMS jitter can achieve 10.35 ps. We easily find the minimum jitter occurs at the shortest pulsewidth.

2-4-2 20 GHz Pulse Train Generation

Fig.2-12 is the pulse train of 20 GHz when MF of 11.000171 GHz. Because of the rational mode-locking, the pulse train is not equalization. The lasing spectrum is shown in Fig. 2-13 and the spectrum spread about 6 nm.

We can record the repetition rate vary with detuning MF in Fig. 2-14. The maximum change range of detuning AL of 16.4 dBm are 0.072 GHz. We can also find the pulsewidth change in Fig. 2-15. The shortest pulsewidth of 21.26 ps is at MF of 11.000169 GHz and AL of 18 dBm. The trend of the change of the rise time in Fig. 2-16 and Fig. 2-17. The shortest rise time is about 4.448 ps at MF of 11.000171 GHz and AL of 16.4 dBm. Following to tuning lower AL and far away 11.000171 GHz, the rise time become more flat. In Fig. 2-17, the trend of falling time is just opposite to rise time. In Fig. 2-18, the RMS jitter has the unregulated variation, but we can find the minimum value of 8.58 ps.

2-4-3 40 GHz Pulse Train Generation

In near the 12 GHz, we can achieve the 40 GHz pulse train. The waveform and optical spectrum are shown in Fig. 2-19 and Fig. 2-20,

respectively. The lasing spectrum is spread over 7 nm. We can use 16.4 dBm to generate repetition rate of 40 GHz by detuning the frequency of 12.000205 GHz. In Fig. 2-21, the variation range of repetition rate of 16.4 dBm are 0.178 GHz. The pulsewidth vary with modulation frequency is shown in Fig. 2-22. We know the shortest pulsewidth is 19.148 ps with AL of 16.4 dBm and MF of 12.000205 GHz. The rise time and falling time depict in Fig. 2-23 and Fig. 2-24. Comparing with above results, there is rise time and falling with MF of 12.000205 GHz GHz and AL of 16.4 dBm. The RMS jitter is shown in Fig. 2-25. The RMS jitter has the optimal value of 5.02 ps.

2-4-4 50 GHz Pulse Train Generation

When the modulation frequency is 12.5 GHz and 16.4 dBm, the 50 GHz pulse train can be generated as shown in Fig. 2-26. Because of limited by sensitivity of oscilloscope, the 50 GHz pulse train is not such clear. The 50 GHz lasing spectrum is shown in Fig. 2-27, we know the lasing spectrum is about 6 nm. In Fig. 2-28, the little variation of repetition rate can be found. We know the maximum value is 50.13 GHz and minimum value is about 49.825 GHz. In Fig. 2-29, we find the narrowest pulsewidth is 13.1 ps. The trend of far away 12.500224 GHz become more broaden. As shown in Fig. 2-30 and Fig. 2-31, the rise time and falling time have the opposite change. We also get the narrowest values of rise time and falling time are 1.148 ps and 1.3 ps, respectively. The RMS jitter has the optimum

value of 5.147 ps at modulation frequency of 12.5002 GHz as shown in Fig. 2-32.

2-5 Summary

In this Chapter, we have demonstrated a new structure of using phase modulated MLF8L. We have trigger the mode-locked laser of repetition rate of 10 GHz, 20 GHz, 40 GHz and 50 GHz with modulation frequency of 10 GHz, 11 GHz, 12 GHz, and 12.5 GHz, respectively. With time-domain ABCD matrix, we budget pulsewidth and chirp parameter of the mode-locked laser cavity. In above experiment, we have known the methods of tuning fitting pulse shape. Besides, we have got RMS jitter of 5.147 ps at modulation frequency of 12.5 GHz. The property of this condition is very beneficial to optical transmission system.

Appendix A

The following martrix derives the dispersion and nonlinear medium. We define the A and B for the real parts of nonlinearity and dispersion, respectively, following as

$$\begin{pmatrix} 1 & 0 \\ iA & 1 \end{pmatrix}\begin{pmatrix} 1 & -iB \\ 0 & 1 \end{pmatrix} \equiv \begin{pmatrix} 1 & 0 \\ i\dfrac{2\gamma \overline{P} L}{N\sqrt{\pi} f \tau^3} & 1 \end{pmatrix}\begin{pmatrix} 1 & -\dfrac{i\beta'' L}{N} \\ 0 & 1 \end{pmatrix} \tag{A-1}$$

$$\mathrm{M} = \begin{pmatrix} 1 & 0 \\ iA & 1 \end{pmatrix}\begin{pmatrix} 1 & -iB \\ 0 & 1 \end{pmatrix} = \begin{pmatrix} 1 & -iB \\ iA & 1+AB \end{pmatrix} \tag{A-2}$$

The characteristic equation is

$$\mathrm{M} - \Omega \mathrm{I} = \begin{pmatrix} 1-\Omega & -iB \\ iA & 1+AB-\Omega \end{pmatrix} \tag{A-3}$$

where I is an unit matrix.

The eigenvalues Ω of (A-2) satisfy

$$\det\left\{\begin{pmatrix} 1-\Omega & -iB \\ iA & 1+AB-\Omega \end{pmatrix}\right\} = \Omega^2 - (AB+2)\Omega + 1 = 0$$

$$\Omega_1 = \frac{AB + 2 + \sqrt{(AB)^2 + 4AB}}{2},$$
$$\Omega_2 = \frac{AB + 2 - \sqrt{(AB)^2 + 4AB}}{2}$$

We use Ω_1 substitution (A-3)

$$\begin{pmatrix} -\frac{AB + \sqrt{(AB)^2 + 4AB}}{2} & -iB \\ iA & \frac{AB - \sqrt{(AB)^2 + 4AB}}{2} \end{pmatrix} \begin{pmatrix} X_1 \\ X_2 \end{pmatrix} = 0 \qquad \text{(A-4)}$$

We know the rank of (A-4) is 1. The eigenvector $\begin{pmatrix} X_1 \\ X_2 \end{pmatrix}$ derive as following

$$-\frac{AB + \sqrt{(AB)^2 + 4AB}}{2} X_1 = iBX_2$$

$$\begin{pmatrix} X_1 \\ X_2 \end{pmatrix} = \begin{pmatrix} i\frac{2B}{AB + \sqrt{(AB)^2 + 4AB}} \\ -1 \end{pmatrix} \qquad \text{(A-5)}$$

We use Ω_2 substitution (A-3)

$$\begin{pmatrix} \dfrac{-AB+\sqrt{(AB)^2+4AB}}{2} & -iB \\ iA & \dfrac{AB+\sqrt{(AB)^2+4AB}}{2} \end{pmatrix} \begin{pmatrix} X_3 \\ X_4 \end{pmatrix} = 0 \qquad \text{(A-6)}$$

$$\frac{-AB+\sqrt{(AB)^2+4AB}}{2} X_3 = iBX_4$$

Another eigenvector is

$$\begin{pmatrix} X_3 \\ X_4 \end{pmatrix} = \begin{pmatrix} i\dfrac{2B}{AB-\sqrt{(AB)^2+4AB}} \\ -1 \end{pmatrix} \qquad \text{(A-7)}$$

From (A-7) and (A-8), we find the model matrix *S* of combining with eigenvectors

$$S = \begin{pmatrix} i\dfrac{2B}{AB+\sqrt{(AB)^2+4AB}} & i\dfrac{2B}{AB-\sqrt{(AB)^2+4AB}} \\ -1 & -1 \end{pmatrix} \qquad \text{(A-8)}$$

The inverse of model matrix is

$$S^{-1} = i\frac{A}{\sqrt{(AB)^2 + 4AB}}\begin{pmatrix} -1 & -i\dfrac{2B}{AB - \sqrt{(AB)^2 + 4AB}} \\ 1 & i\dfrac{2B}{AB + \sqrt{(AB)^2 + 4AB}} \end{pmatrix} \qquad \text{(A-9)}$$

In accordance with diagonal theorem, we derive the diagonal matrix as following

$$D = S^{-1}\mathrm{M}S$$

$$= i\frac{A}{\sqrt{(AB)^2 + 4AB}}\begin{pmatrix} -1 & -i\dfrac{2B}{AB - \sqrt{(AB)^2 + 4AB}} \\ 1 & i\dfrac{2B}{AB + \sqrt{(AB)^2 + 4AB}} \end{pmatrix} \times$$

$$\begin{pmatrix} 1 & -iB \\ iA & 1 + AB \end{pmatrix} \times$$

$$\begin{pmatrix} i\dfrac{2B}{AB + \sqrt{(AB)^2 + 4AB}} & i\dfrac{2B}{AB - \sqrt{(AB)^2 + 4AB}} \\ -1 & -1 \end{pmatrix} \qquad \text{(A-10)}$$

$$\equiv \begin{pmatrix} U & 0 \\ 0 & V \end{pmatrix}$$

where

$$U = 1 + \frac{1}{2}AB + \frac{\frac{1}{2}(AB)^2 + 2AB}{AB + \sqrt{(AB)^2 + 4AB}} \tag{A-11}$$

$$V = 1 + \frac{1}{2}AB - \frac{\frac{1}{2}(AB)^2 + 2AB}{AB + \sqrt{(AB)^2 + 4AB}} \tag{A-12}$$

From (A-2), (A-8) and (A-9), we solve the matrix M of N order as

$$\mathrm{M}^N = SD^N S^{-1}$$

$$= \begin{pmatrix} i\dfrac{2B}{AB + \sqrt{(AB)^2 + 4AB}} & i\dfrac{2B}{AB - \sqrt{(AB)^2 + 4AB}} \\ -1 & -1 \end{pmatrix} \times$$

$$\begin{pmatrix} U^N & 0 \\ 0 & V^N \end{pmatrix} \times$$

$$i\frac{A}{\sqrt{(AB)^2 + 4AB}} \begin{pmatrix} -1 & -i\dfrac{2B}{AB - \sqrt{(AB)^2 + 4AB}} \\ 1 & i\dfrac{2B}{AB + \sqrt{(AB)^2 + 4AB}} \end{pmatrix}$$

$$\equiv \begin{pmatrix} W & X \\ Y & Z \end{pmatrix} \tag{A-13}$$

where

$$W = \frac{A}{\sqrt{(AB)^2 + 4AB}} \left(\frac{2B}{AB + \sqrt{(AB)^2 + 4AB}} U^N - \frac{2B}{AB - \sqrt{(AB)^2 + 4AB}} V^N \right)$$

(A-14)

$$X = i \frac{B}{\sqrt{(AB)^2 + 4AB}} \left(-U^N + V^N \right)$$

(A-15)

$$Y = i \frac{A}{\sqrt{(AB)^2 + 4AB}} \left(U^N - V^N \right)$$

(A-16)

$$Z = \frac{-A}{\sqrt{(AB)^2 + 4AB}} \left(\frac{2B}{AB - \sqrt{(AB)^2 + 4AB}} U^N - \frac{2B}{AB + \sqrt{(AB)^2 + 4AB}} V^N \right)$$

(A-17)

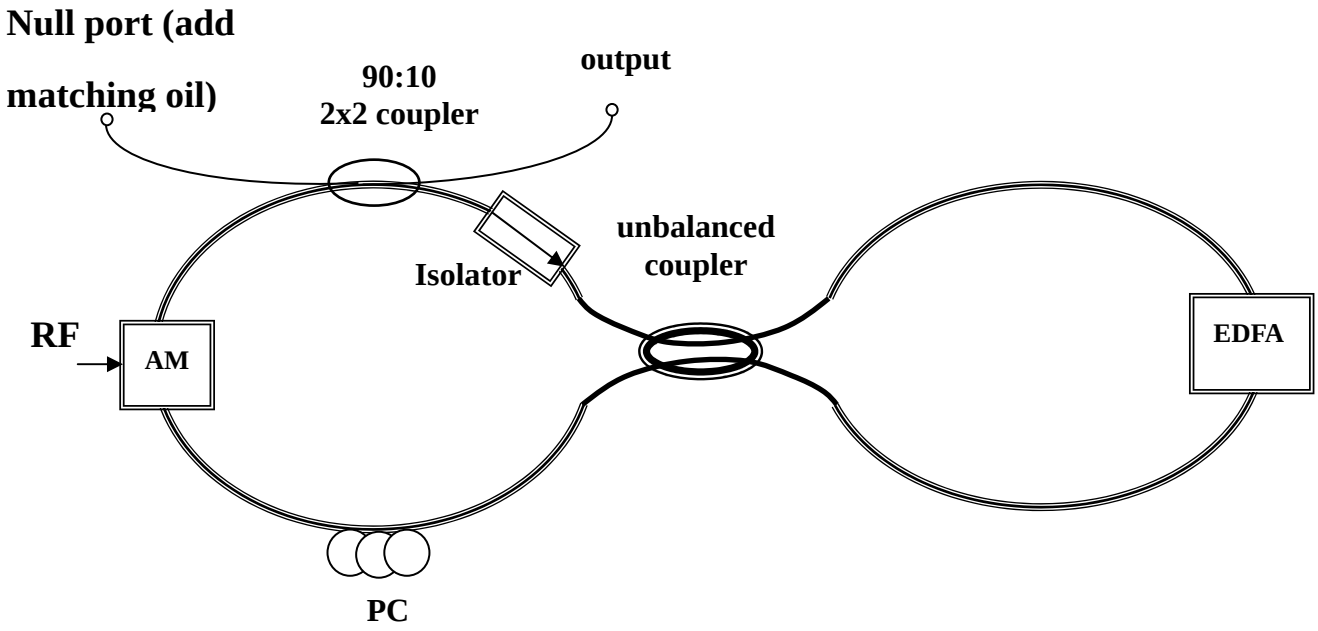

Fig. 2-1 The structure of an amplitude-modulated MLF8L

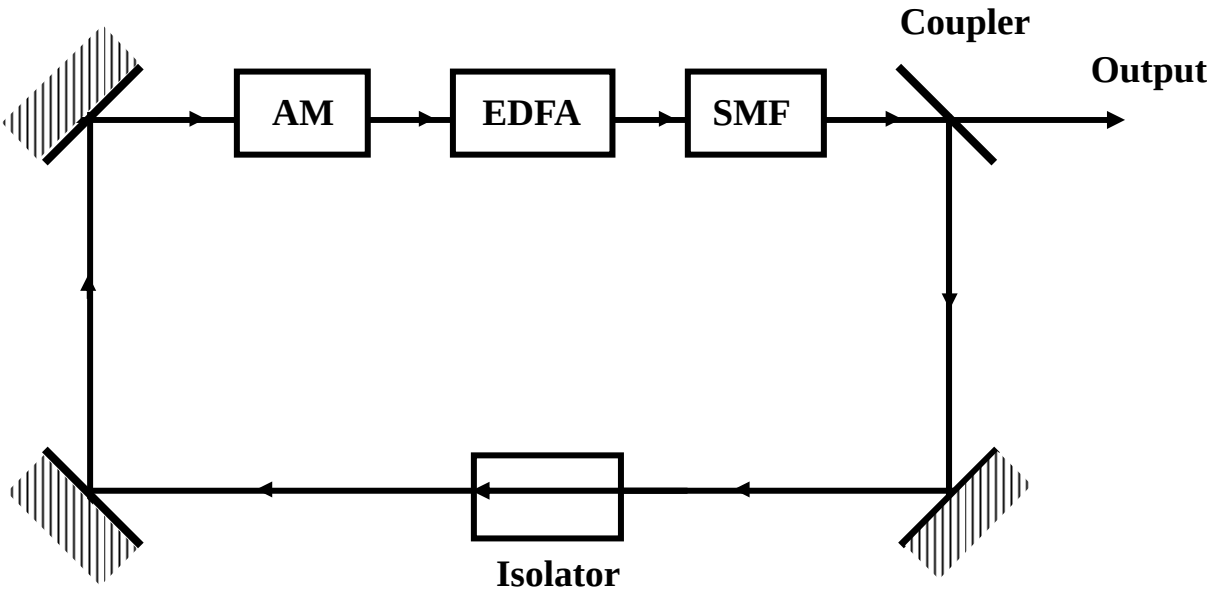

Fig. 2-2 The schematic expressions of the MLF8L using time-domain ABCD matrix

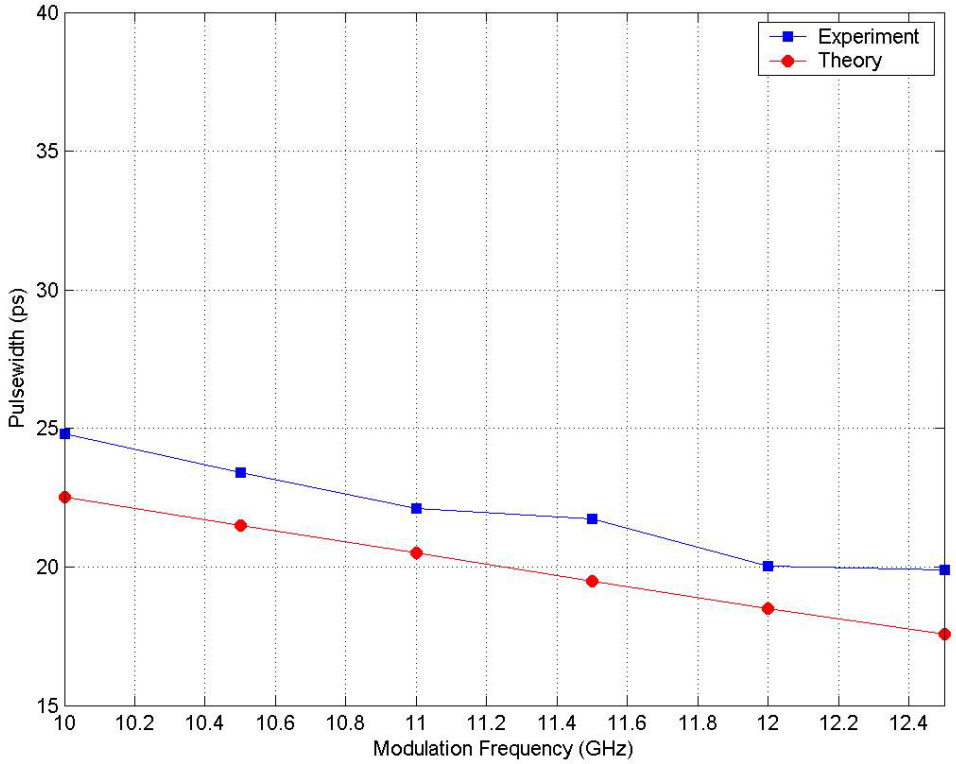

Fig. 2-3 The diagram of comparing with theory and experiment

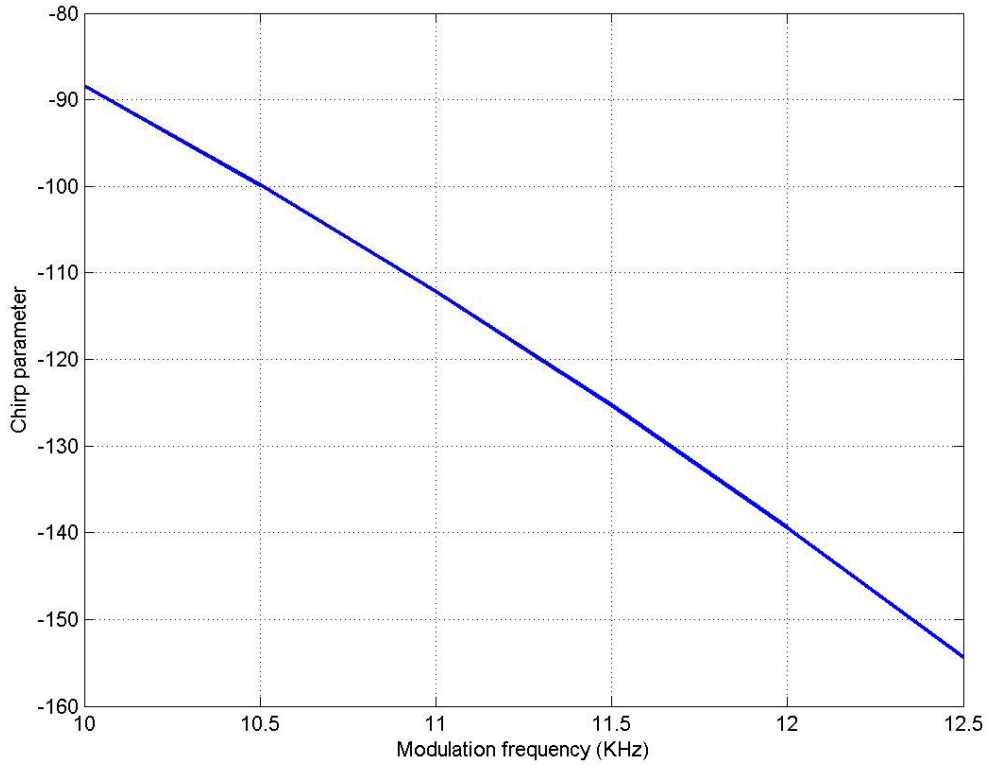

Fig. 2-4 The chirp parameter change with modulation frequency

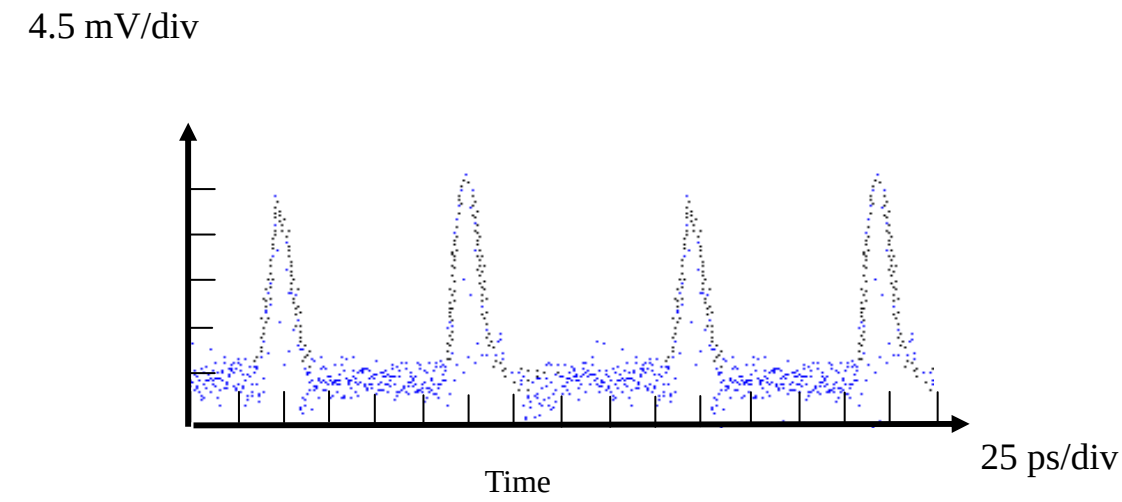

Fig. 2-5 The pulse train of MLF8L with modulation frequency of 10 GHz and amplitude level of 16.4 dBm

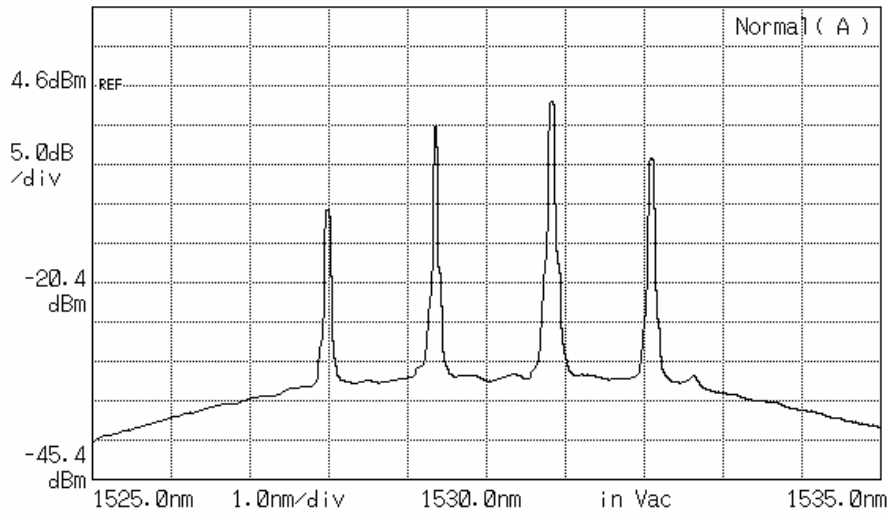

Fig. 2-6 The 10 GHz lasing spectrum with modulation frequency of 10 GHz and amplitude level of 16.4 dBm

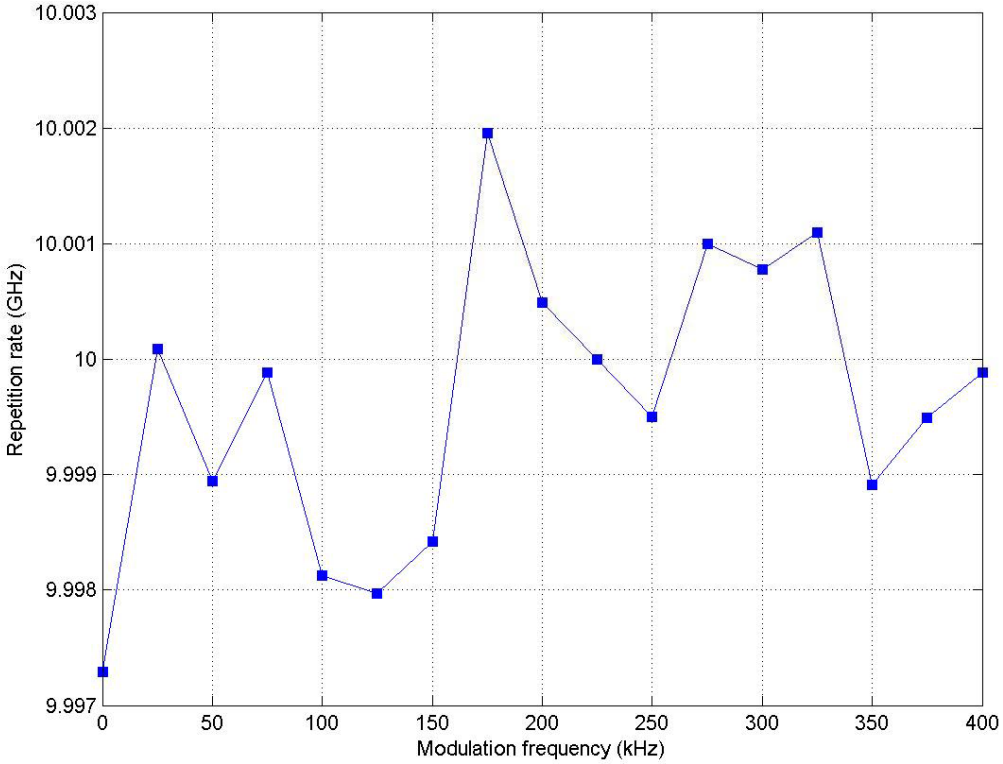

Fig. 2-7 Change of repetition rate by detuning modulation frequency (Offset=10GHz)

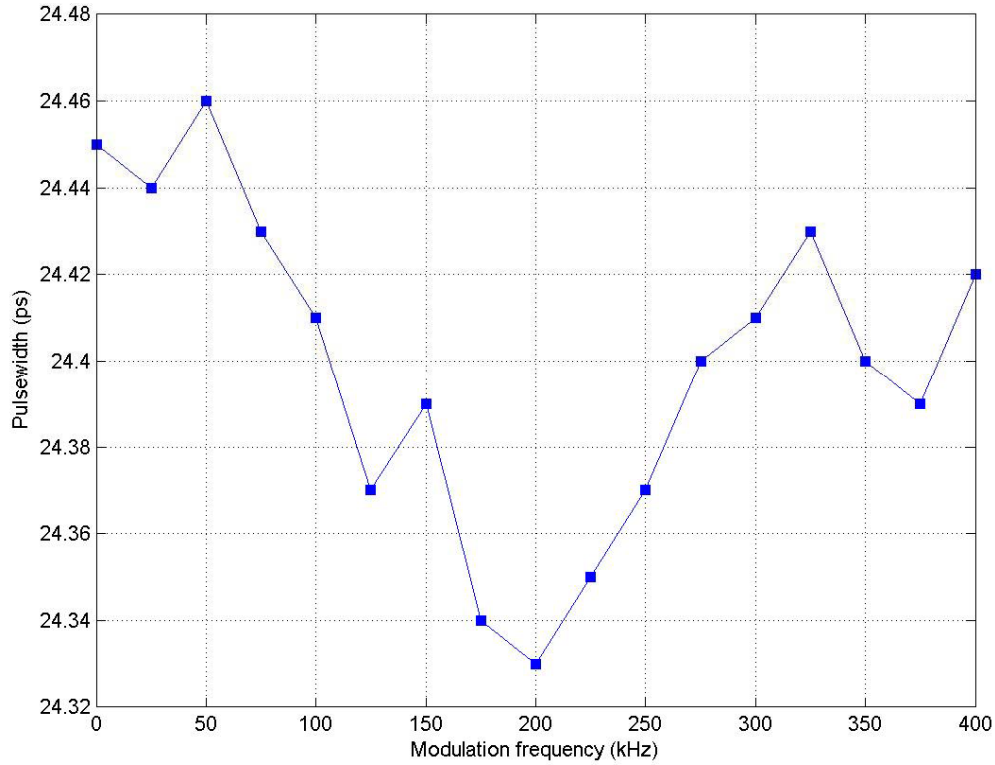

Fig. 2-8 Variation of pulsewidth by detuning modulation frequency (Offset=10GHz)

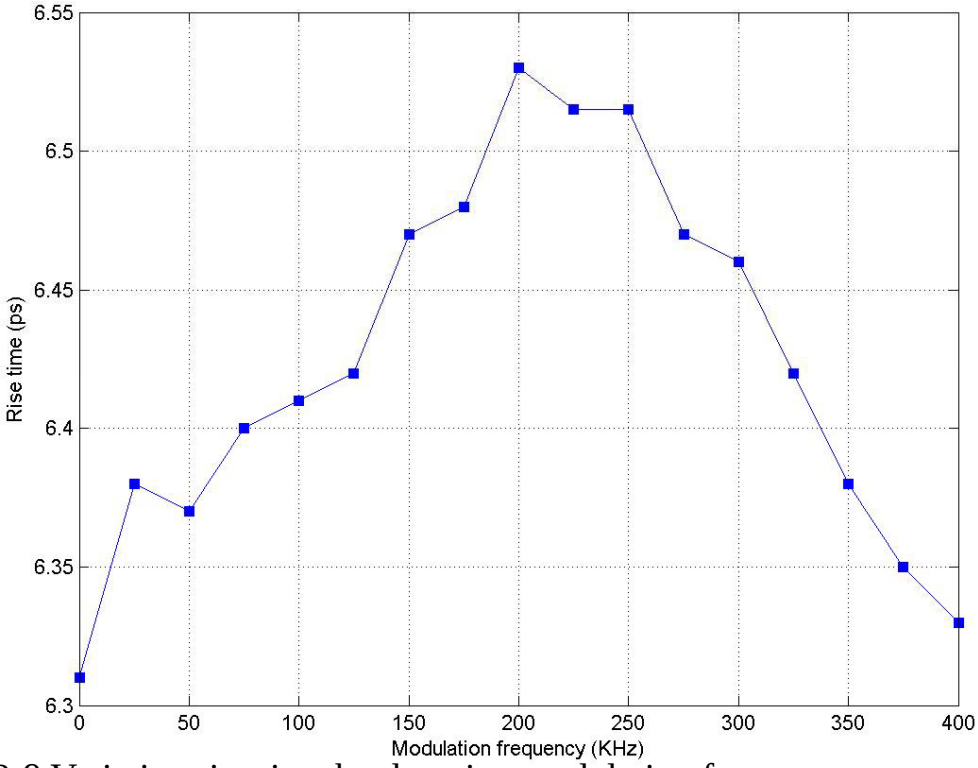

Fig. 2-9 Variation rise time by detuning modulation frequency (Offset=10GHz)

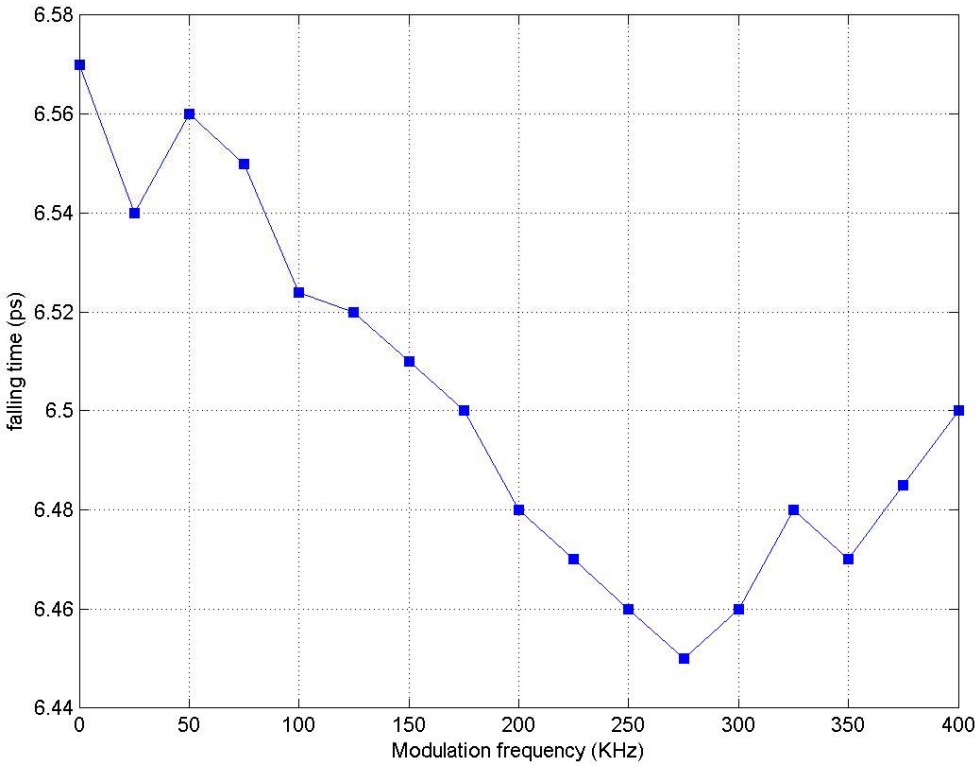

Fig. 2-10 Variation of falling time by detuning modulation frequency (Offset=10GHz)

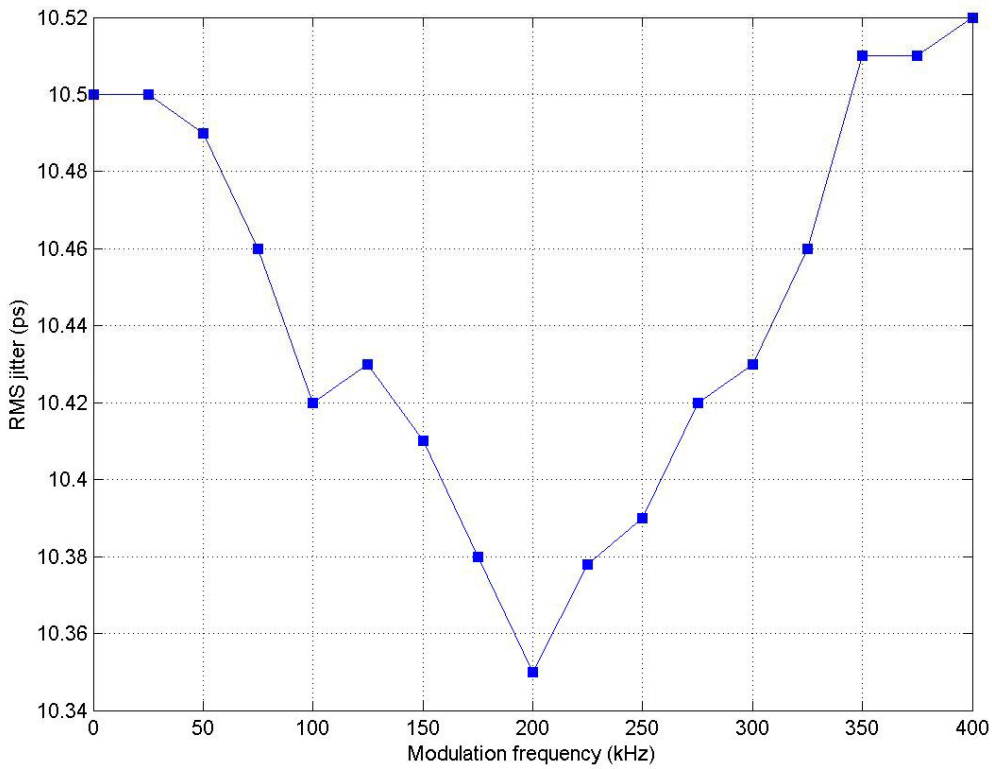

Fig. 2-11 Variation of RMS jitter by detuning modulation frequency (Offset=10GHz)

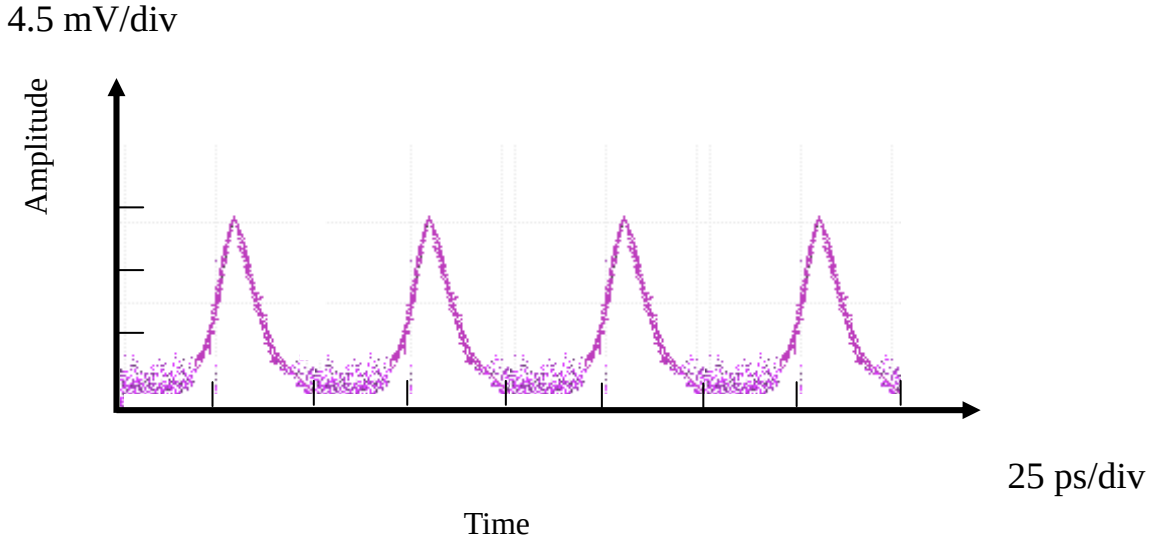

Fig. 2-12 The pulse train of MLF8L with modulation frequency of 11 GHz and amplitude level of 16.4 dBm

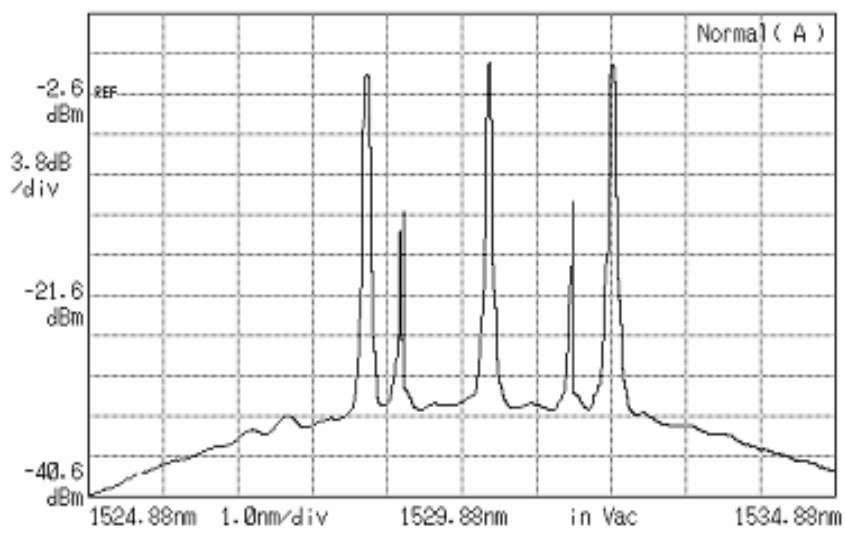

Fig. 2-13 The 20 GHz lasing spectrum with modulation frequency of 11 GHz and amplitude level of 16.4 dBm

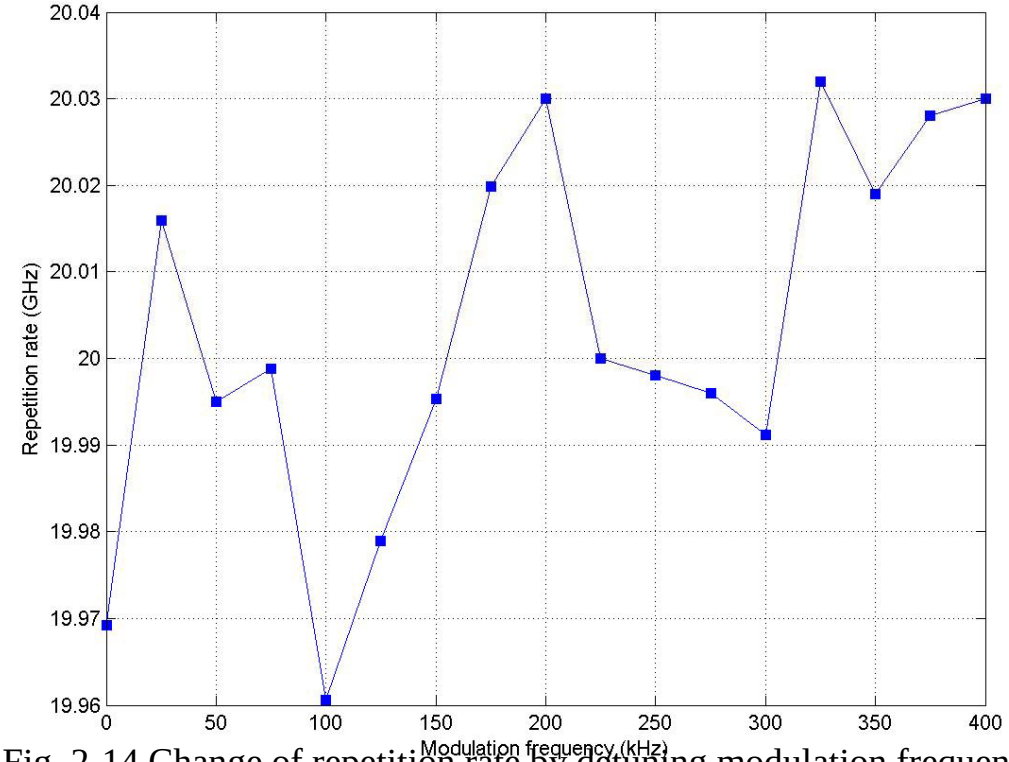

Fig. 2-14 Change of repetition rate by detuning modulation frequency (Offset=11.0GHz)

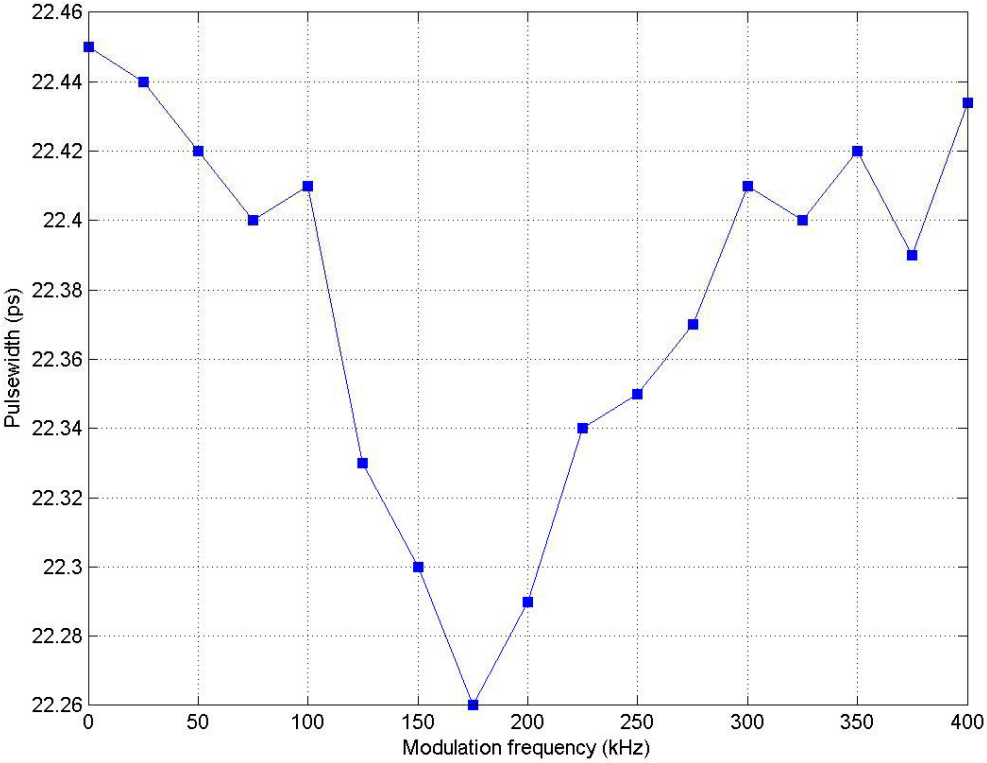

Fig. 2-15 Variation of pulsewidth by detuning modulation frequency (Offset=11.0GHz)

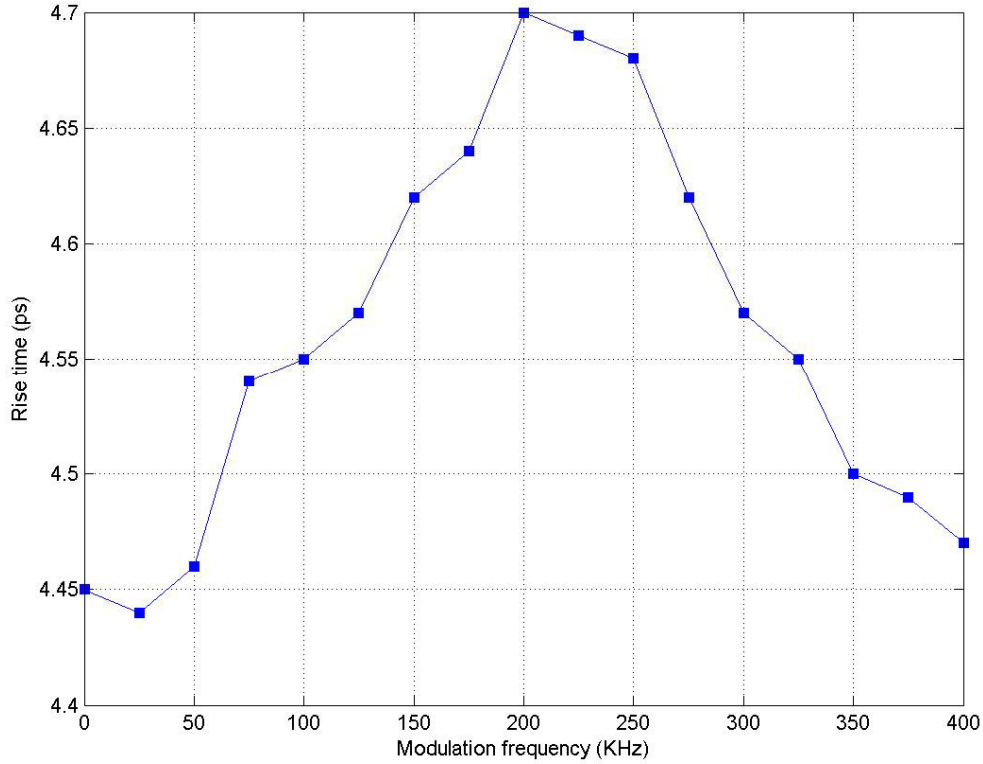

Fig. 2-16 Variation of rise time by detuning modulation frequency (Offset=11.0GHz)

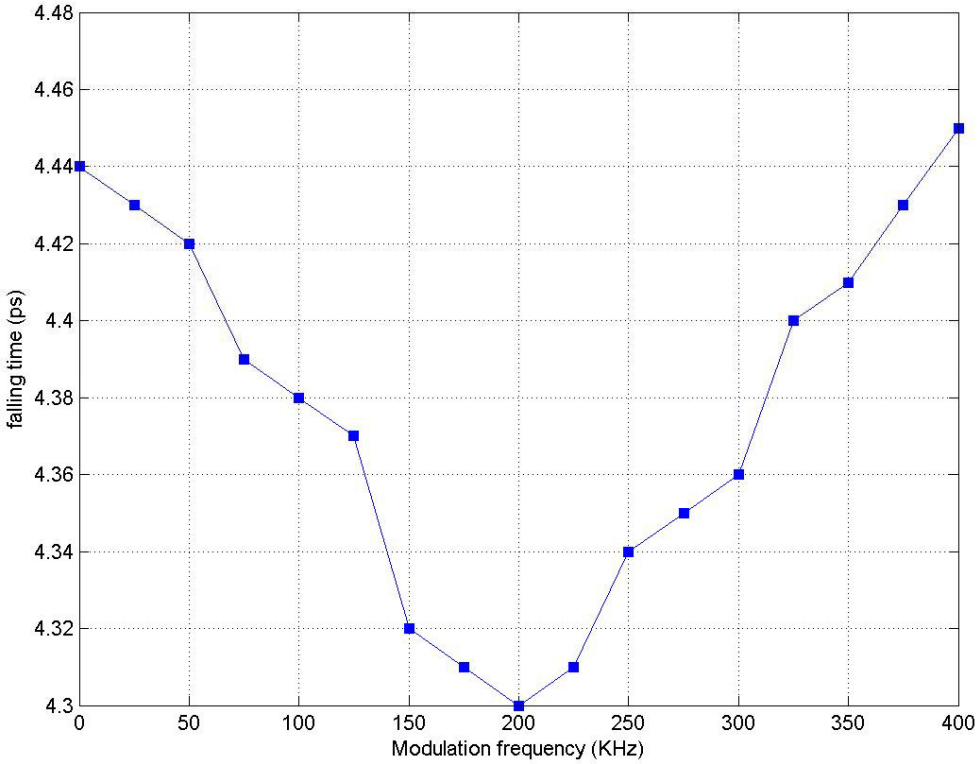

Fig. 2-17 Variation of falling time by detuning modulation frequency (Offset=11.0GHz)

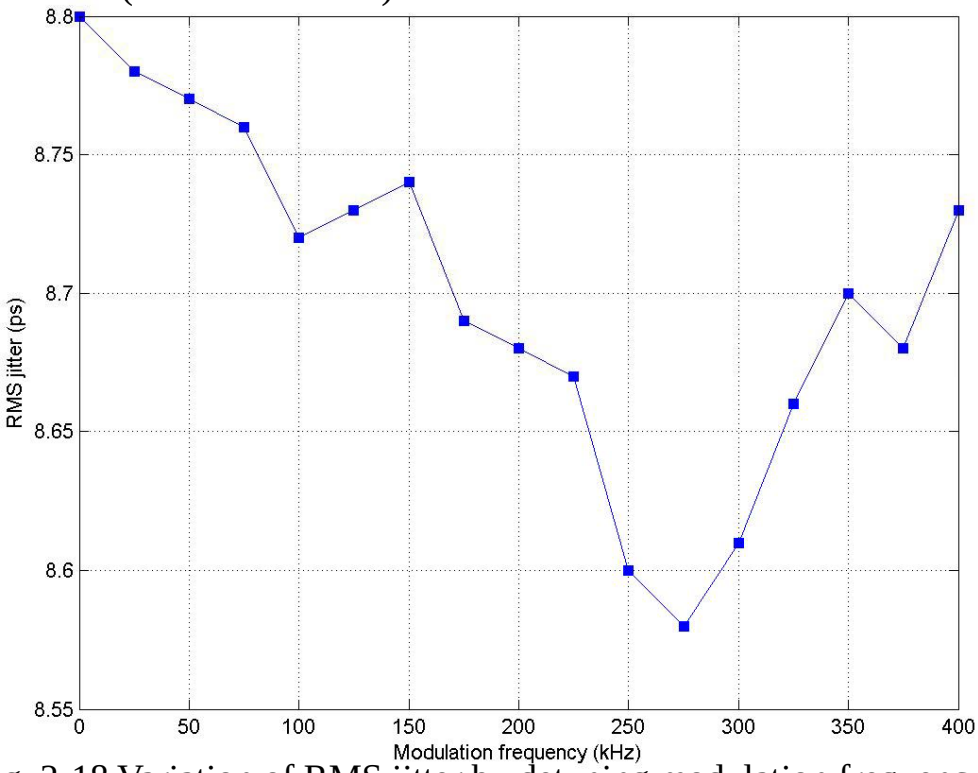

Fig. 2-18 Variation of RMS jitter by detuning modulation frequency (Offset=11.0GHz)

4.5 mV/div

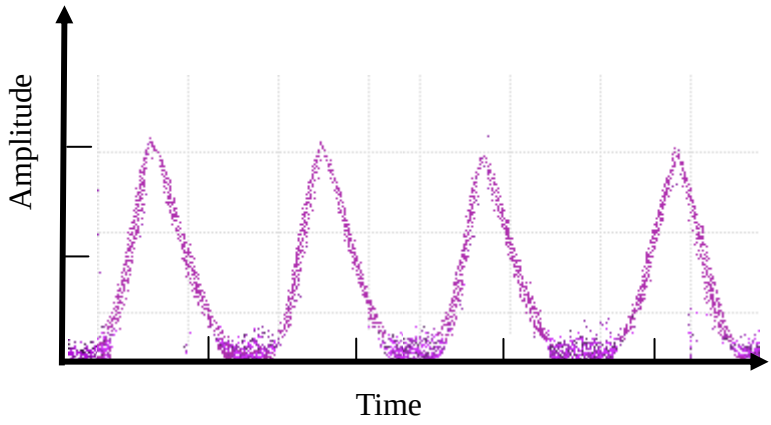

25 ps/div

Fig. 2-19 The 40 GHz pulse train of MLF8L with modulation frequency of 12 GHz and amplitude level of 16.4 dBm

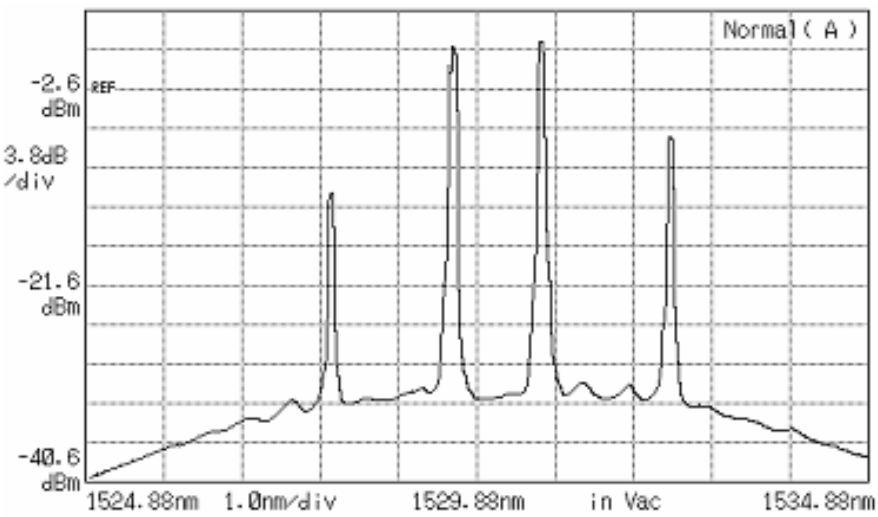

Fig. 2-20 The 40 GHz lasing spectrum with modulation frequency of 12 GHz and amplitude level of 16.4 dBm

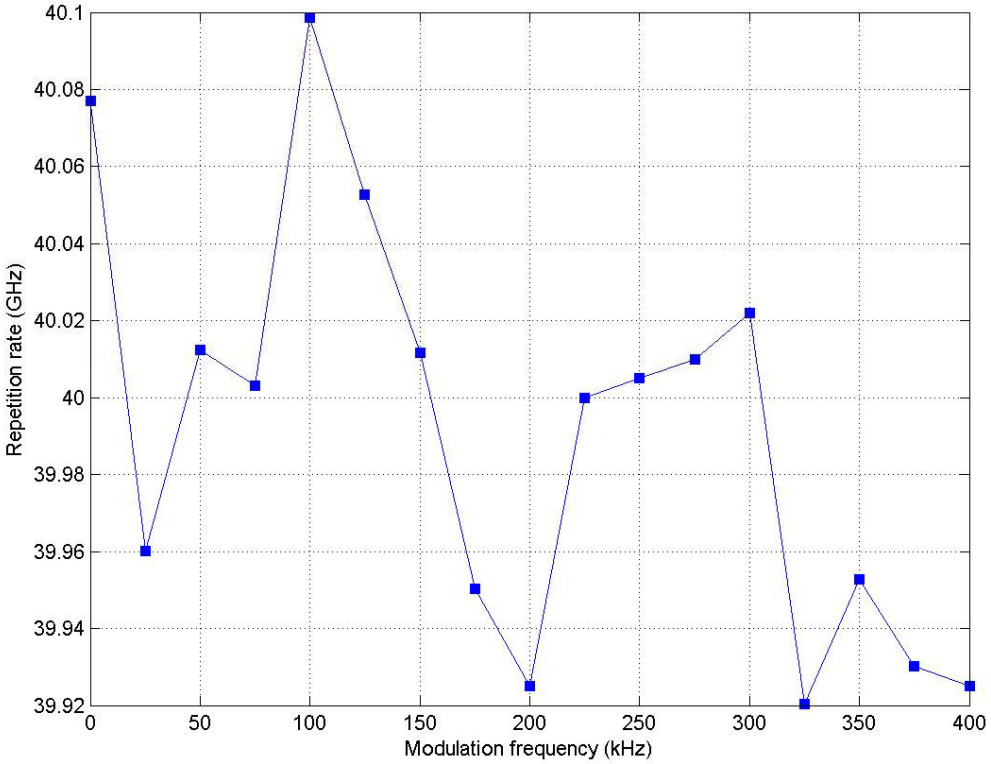

Fig. 2-21 Change of repetition rate by detuning modulation frequency (Offset=12.0GHz)

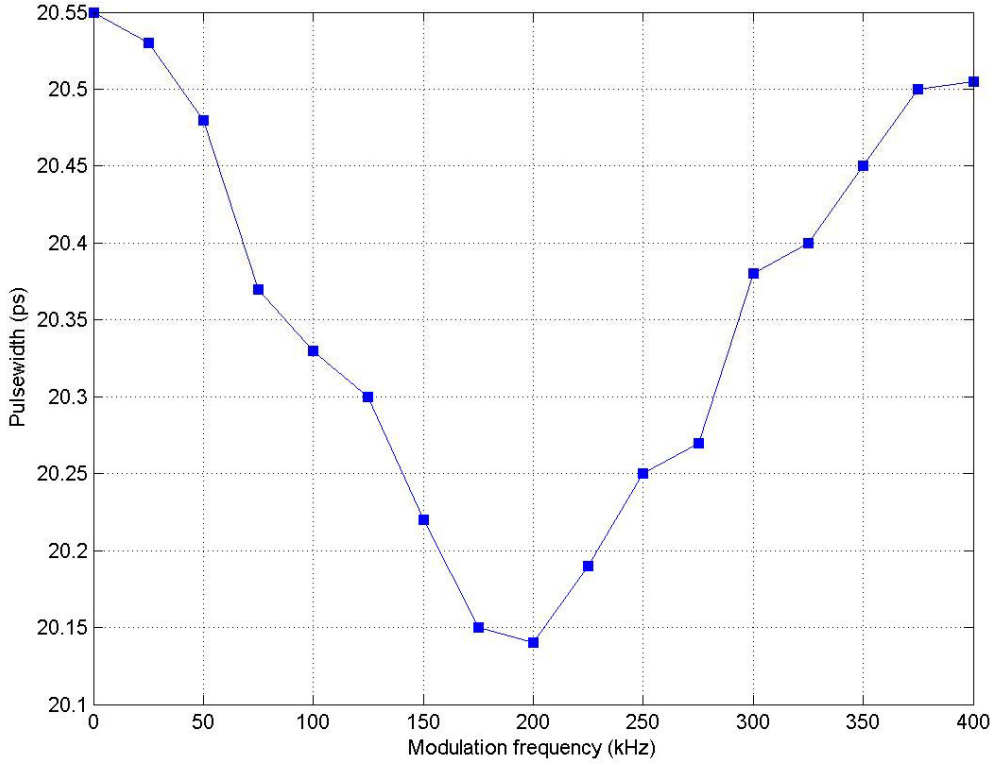

Fig. 2-22 Variation of pulsewidth by detuning modulation frequency (Offset=12.0GHz)

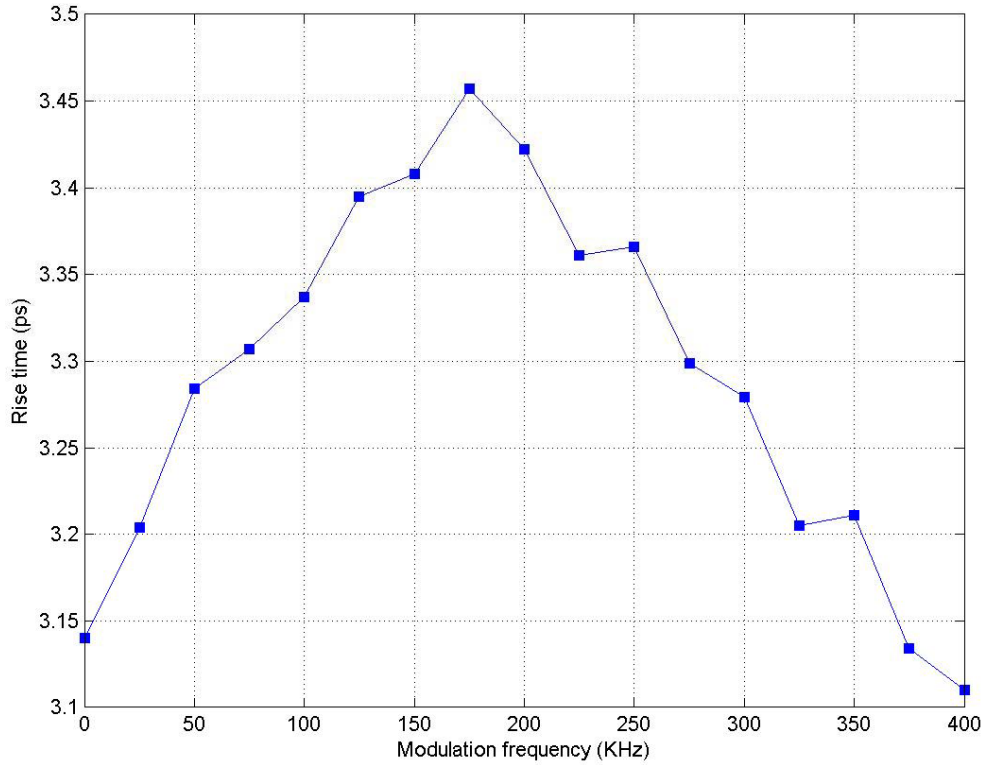

Fig. 2-23 Variation of rise time by detuning modulation frequency

(Offset=12.0GHz)

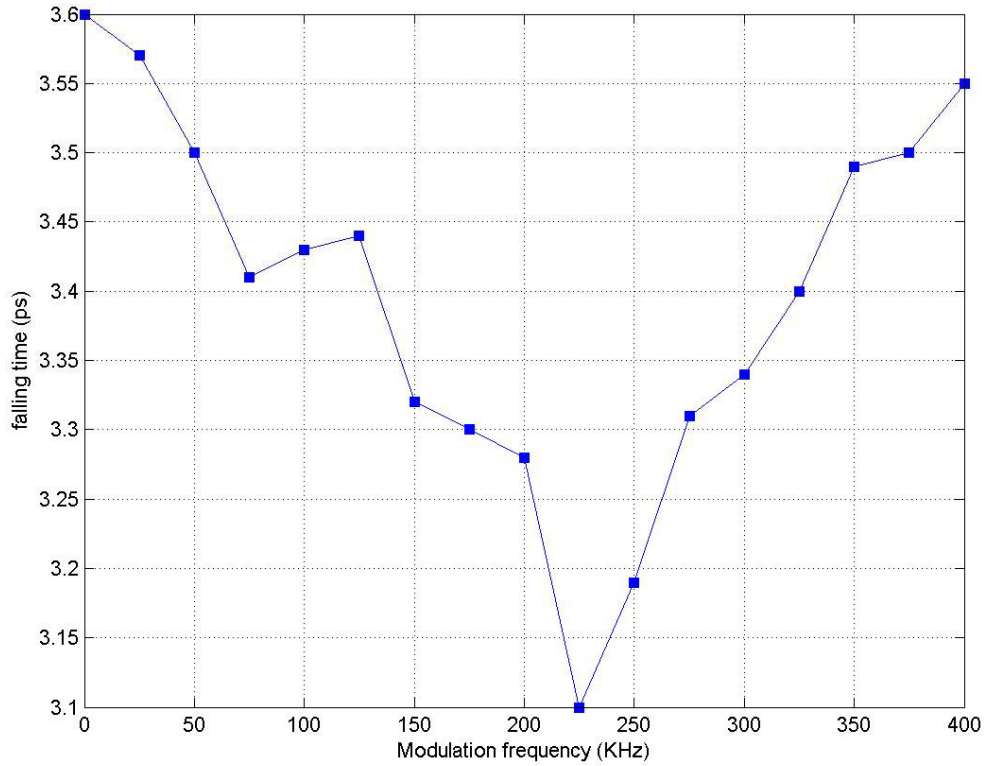

Fig. 2-24 Variation of falling time by detuning modulation frequency

(Offset=12.0GHz)

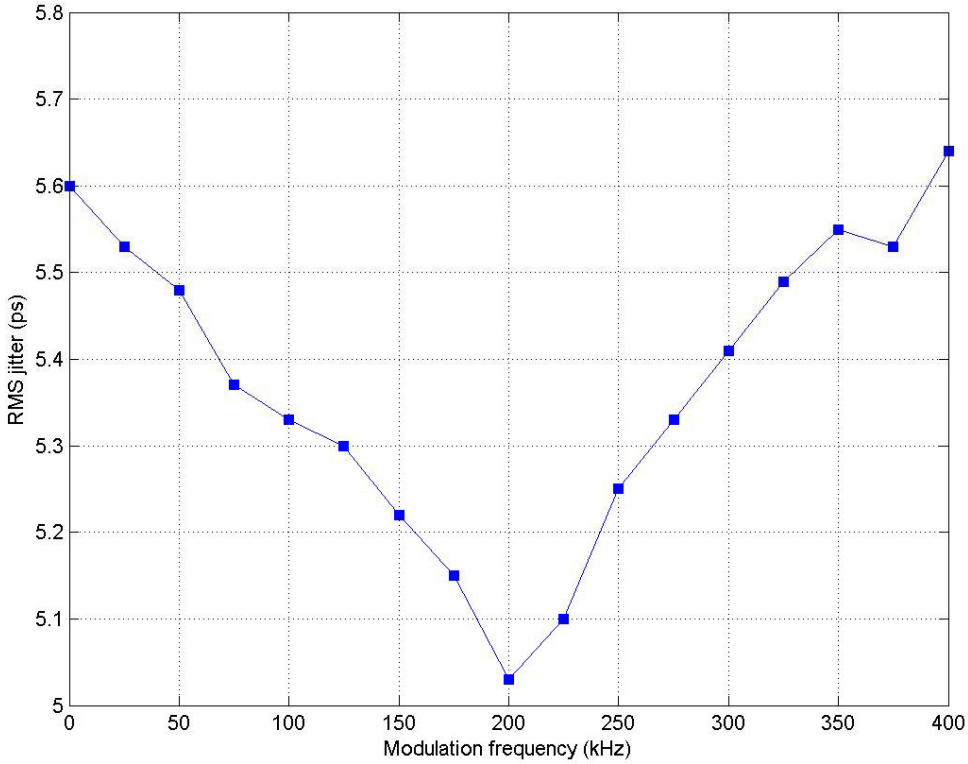

Fig. 2-25 Variation of RMS jitter by detuning modulation frequency (Offset=12.0GHz)

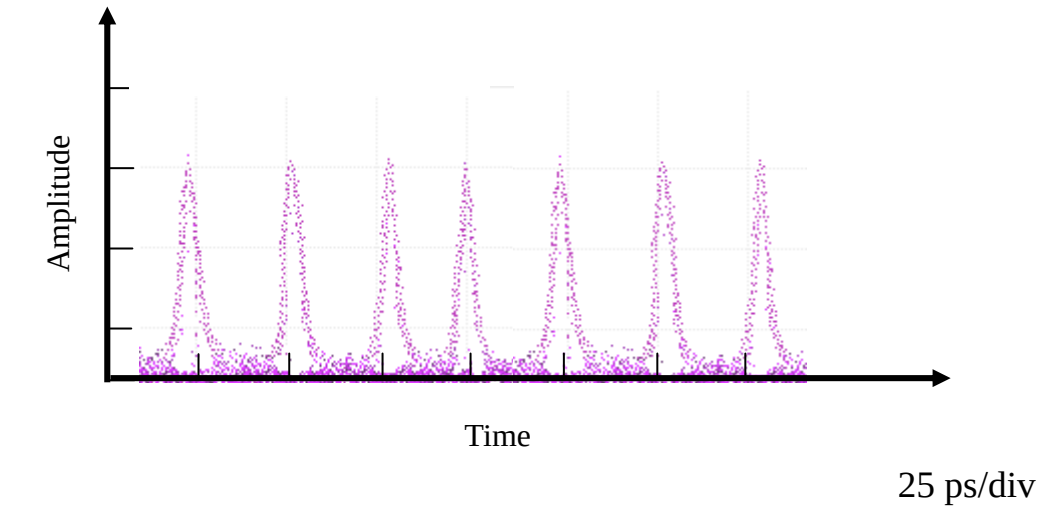

Fig. 2-26 The 50 GHz mode-locked pulse train with modulation frequency of 12.5 GHz and amplitude level of 16.4 dBm

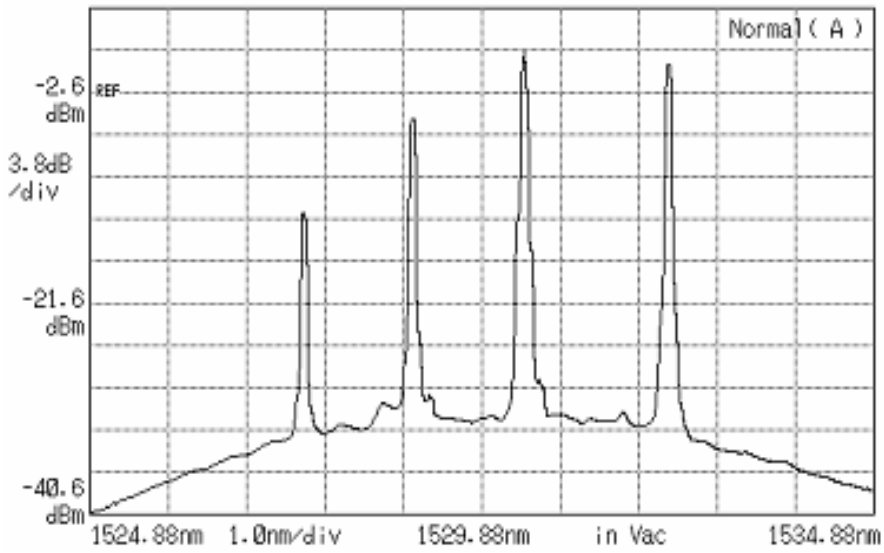

Fig. 2-27 The 50 GHz lasing spectrum with modulation frequency of 12.5 GHz and amplitude level of 16.4 dBm

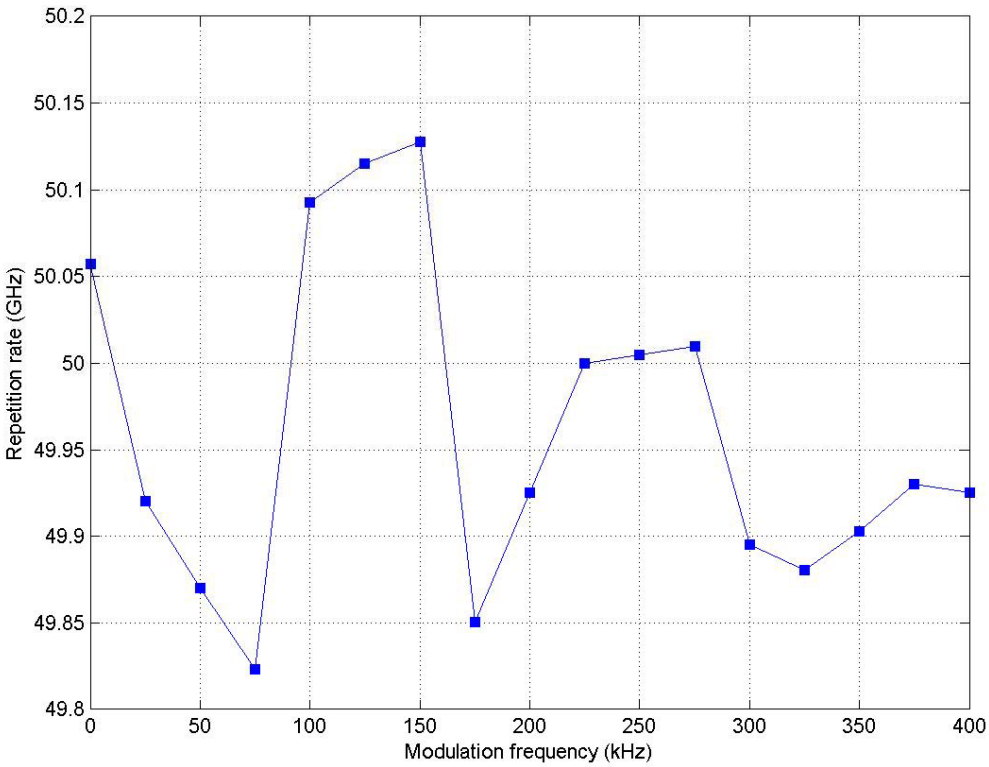

Fig. 2-28 Change of repetition rate by detuning modulation frequency (Offset=12.5GHz)

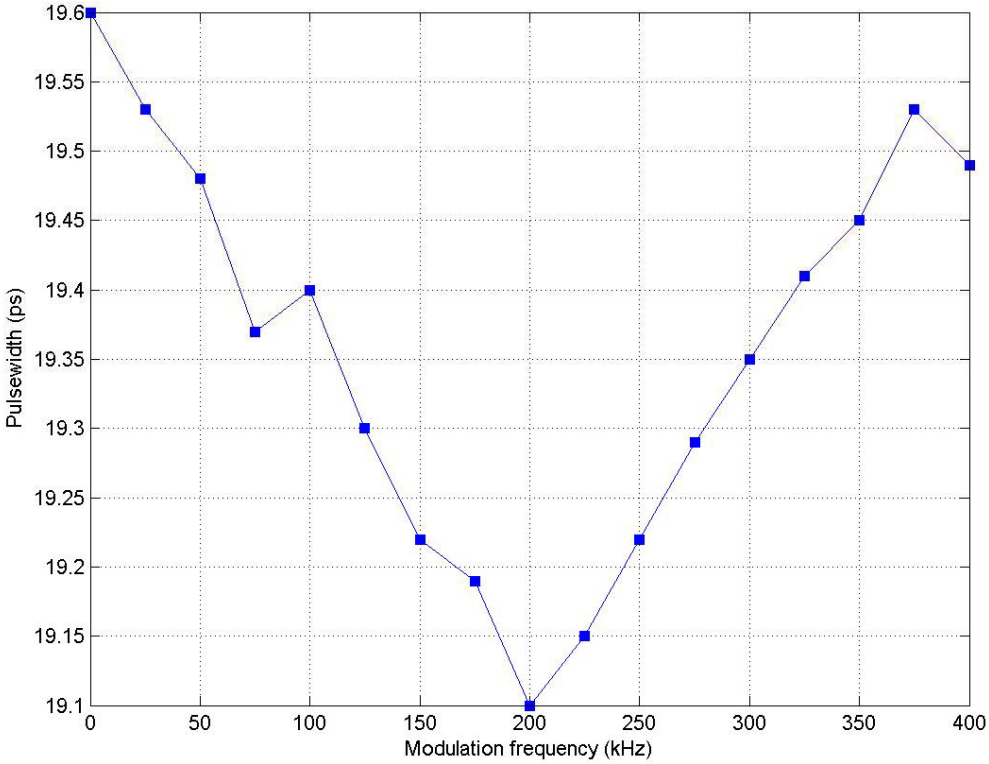

Fig. 2-29 Change of pulsewidth by detuning modulation frequency (Offset=12.5GHz)

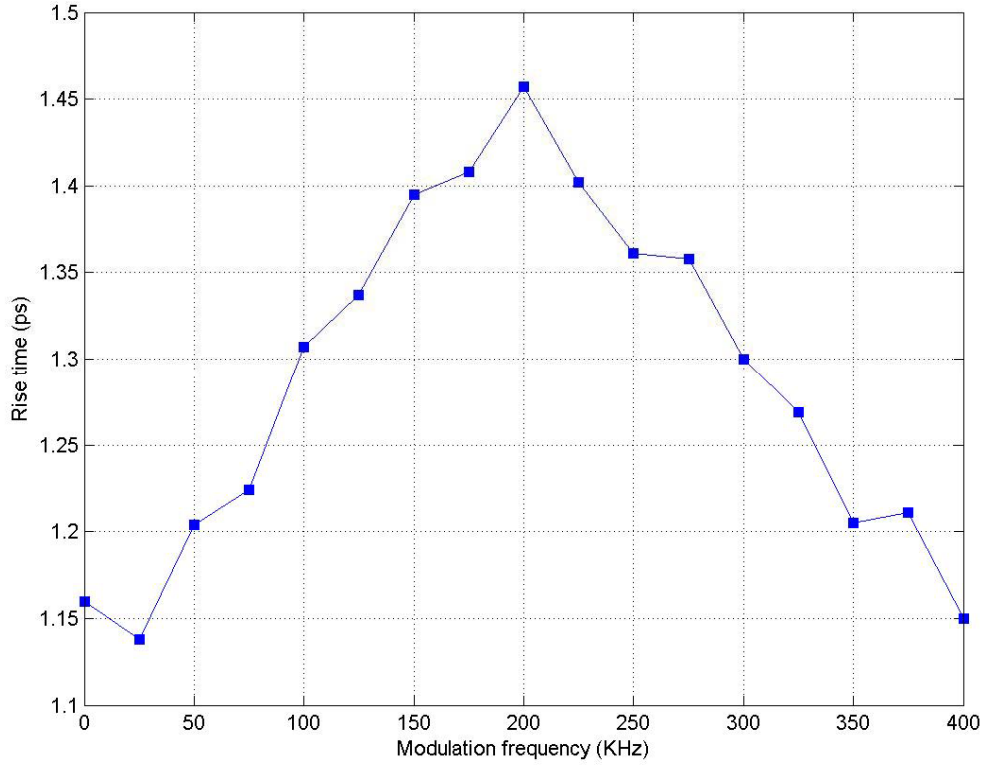

Fig. 2-30 Variation of rise time by detuning modulation frequency (Offset=12.5GHz)

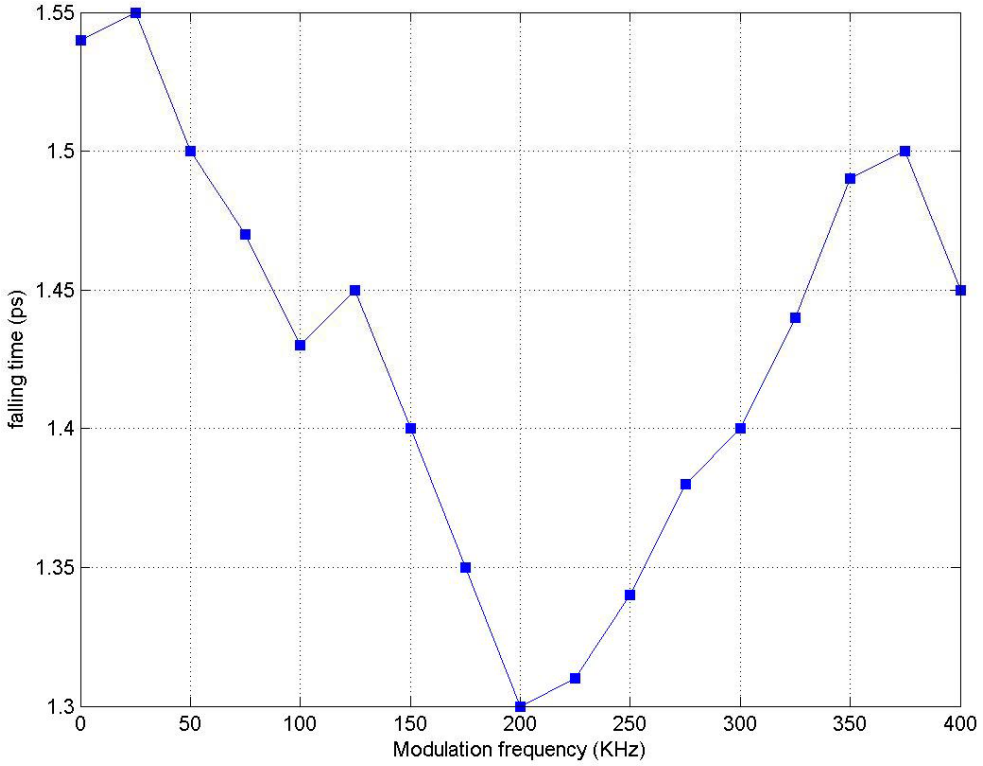

Fig. 2-31 Variation of falling time by detuning modulation frequency (Offset=12.5GHz)

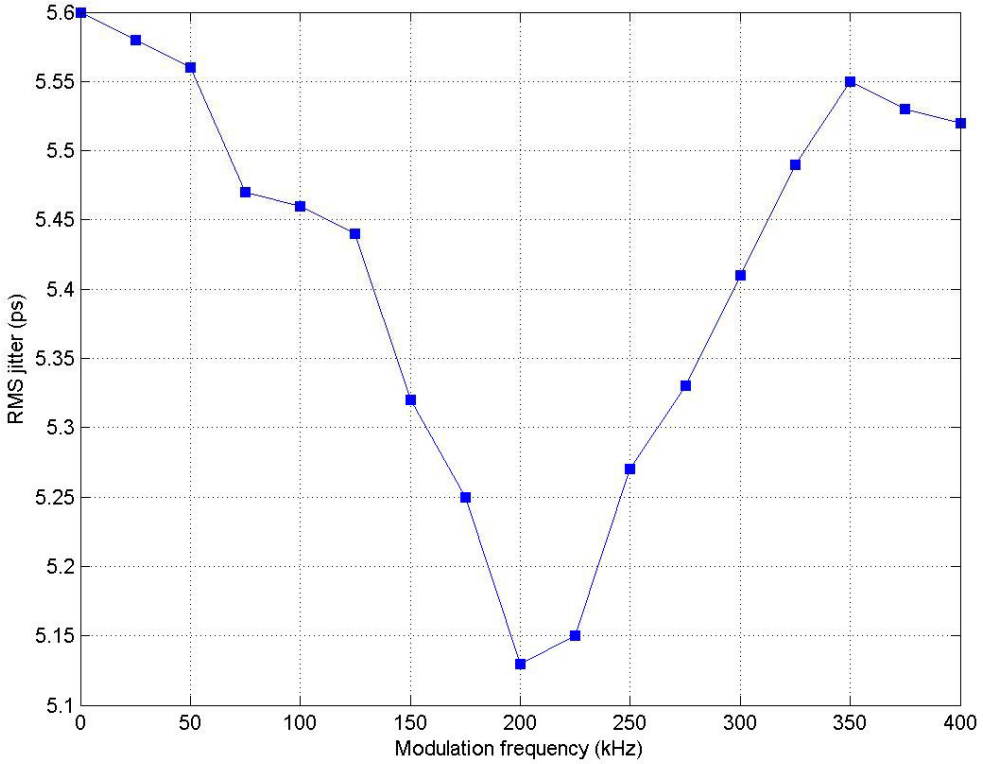

Fig. 2-32 Variation of RMS jitter by detuning modulation frequency (Offset=12.5GHz)

Table 2-1

	Elements	Time Domain ABCD Matrix
1	Amplitude modulator	$\begin{pmatrix} 1 & 0 \\ 4\pi^2 m f^2 & 1 \end{pmatrix}$
2	SMF with dispersion	$\begin{pmatrix} 1 & -i\beta_S'' L_S \\ 0 & 1 \end{pmatrix}$
3	SMF with nonlinearity	$\begin{pmatrix} 1 & 0 \\ i\frac{2\gamma_S \overline{P} L_S}{\sqrt{\pi} f \tau^3} & 1 \end{pmatrix}$
4	EDF with dispersion	$\begin{pmatrix} 1 & -i\beta_E'' L_E \\ 0 & 1 \end{pmatrix}$
5	EDF with nolinearity	$\begin{pmatrix} 1 & 0 \\ i\frac{2\gamma_E \overline{P} L_E}{\sqrt{\pi} f \tau^3} & 1 \end{pmatrix}$

Table 2-2

Parameter	Symbol	Value
Second-order dispersion of SMF	β_S''	-1.86x10^{-26} sec^2/m
Second-order dispersion of EDF	β_E''	-1.46x10^{-26} sec^2/m
Length of SMF	L_S	64.19 m
Length of EDF	L_E	9 m
Nonlinear coefficient of SMF	γ_S	0.002 (m・W)$^{-1}$
Nonlinear coefficient of EDF	γ_E	0.02 (m・W)$^{-1}$
Average power	$\overline{P}$	1.275 mW
Modulation depth	m	0.001
Modulation frequency	f	10GHz~12.5 GHz
Split number of EDF	M	100
Split number of SMF	N	100